

Article

Investigation of the Microstructure and Mechanical Properties in Friction Stir Welded Dissimilar Aluminium Alloy Joints via Sampling Direction

Sipokazi Mabuwa *  and Velaphi Msomi 

Mechanical and Mechatronic Engineering Department, Cape Peninsula University of Technology, Bellville 7535, South Africa; msomiv@gmail.com

* Correspondence: sipokazimabuwa@gmail.com; Tel.: +27-219-538-778

Abstract: This research study investigates the influence of sampling direction on the microstructure and mechanical properties of dissimilar joints formed by friction stir welding (FSW). The specimens were cut in two directions: perpendicular (transverse) and parallel (longitudinal) to the FSW joint. The tests conducted included X-ray diffraction (XRD), macrostructure, microstructure, tensile, microhardness, and fractography analysis. Different phases were noted in the XRD patterns and explained, with the aluminum phase being the dominating one. The results further showed that the transverse dissimilar joint exhibited higher microhardness compared to the longitudinal dissimilar joint, which is consistent with the respective grain sizes. Moreover, the ultimate tensile strength of the longitudinal joint exceeded that of the transverse joints, showing a substantial 47% increase. Similarly, the elongation of the joints followed a similar trend, with the longitudinal joint displaying a significant 41% increase in elongation compared to the transverse joint. Fractographic analysis revealed ductile fracture behaviour in all joints.

Keywords: X-ray diffraction patterns; dissimilar aluminum alloys; tensile strength; microstructure



Citation: Mabuwa, S.; Msomi, V. Investigation of the Microstructure and Mechanical Properties in Friction Stir Welded Dissimilar Aluminium Alloy Joints via Sampling Direction. *Crystals* **2023**, *13*, 1108. <https://doi.org/10.3390/cryst13071108>

Academic Editors: Ali Khalfallah, Mahmoud Moradi and Reza Beygi

Received: 29 June 2023
Revised: 9 July 2023
Accepted: 13 July 2023
Published: 16 July 2023



Copyright: © 2023 by the authors. Licensee MDPI, Basel, Switzerland. This article is an open access article distributed under the terms and conditions of the Creative Commons Attribution (CC BY) license (<https://creativecommons.org/licenses/by/4.0/>).

1. Introduction

Friction stir welding (FSW) is defined as a solid-state joining technique whereby the welding process is performed below the materials melting temperature in a solid state [1]. The FSW technique was initially invented and designed for aluminum alloys by The Welding Institute (TWI) in the United Kingdom in 1991 [1,2]. Since then, the FSW technique has been normalized as a joining technique for other materials such as steel, titanium, copper, and magnesium. The application of FSW advanced into many applications, including the joining of dissimilar materials. The weld characteristics of the dissimilar FSW materials were discovered to be influenced mainly by welding parameters. Welding parameters refer to the FSW machine parameters, which include rotational speed, traverse speed, axial force, tool tilt angle, vertical force, and tool parameters such as the material of the tool, shoulder diameter, pin length, pin diameter, and pin profile [3].

There are many studies where FSW was successfully employed to join dissimilar materials, including dissimilar aluminum alloys. The AA6063 and AA7075 dissimilar aluminum alloy joint was produced using FSW to investigate the microstructure and mechanical properties of the produced joint [4]. Varying process parameters were used, and it was discovered that the sound results were obtained when the tool rotation was set at 1000 rpm and a traverse speed of 2.5 mm/s with an axial force of 8.5 kN. The results reported included the fine-grained microstructure, which was found to be responsible for the high hardness and tensile strength. A dissimilar combination of AA2024 and AA7075 was subject to FSW to evaluate the impact of welding parameters using varying parameters [5]. The varying parameters included a tool rotation range of 1000–1400 rpm, a tool traverse speed range of 20–40 mm/min, and a constant force of 4 kN. The ultimate

tensile strength (UTS) was found to increase with a decrease in traverse speed, while the microstructural grain patterns were found to coarsen as the tool rotation increased due to high heat input in the deformed zone. In addition, Kailainathan et al. [6] reported a similar behavior where the UTS depreciated when the tool rotation was above 1200 rpm. This was due to the distortion in the weld region caused by the severe heat experience by the welded region during FSW.

The material positioning is considered to be crucial during the FSW of dissimilar aluminum alloys. Guo et al. [7] combined varying process parameters and material positioning to determine the impact the two factors had on the produced AA6061/AA7075 dissimilar joint characteristics. The microstructure results revealed that the material mixing was more effective when the AA6061 alloy was placed on the advancing side than when the AA7075 was positioned on the advancing side. Greater grain refinement was also found to favor the positioning of the same alloy on the advancing side. The highest UTS was obtained under the exact positioning at a high traverse speed of 5 mm/s.

To investigate the impact of material positioning and tool offset, researchers conducted a friction stir welding experiment using AA6061-T6 and AA8011-H14, as detailed in Reference [8]. The welding process involved specific parameters, including a tool rotational speed of 1070 rpm, a tool traverse speed of 50 mm/min, and a tool tilt angle of 2°. By placing the softer AA8011-H14 alloy on the advancing side of the tool, with a tool offset of 1 mm, notable improvements were achieved in the joint properties. The tensile test results revealed a maximum UTS of 77.8 MPa and an elongation of 21.96%. However, the hardness remained unaffected by the varying process parameters. The weld zone exhibited a consistent grain structure. Additionally, various studies in the literature, spanning from References [9–12], have corroborated the idea of positioning the softer material on the advancing side of the tool, irrespective of the specific combinations of dissimilar aluminum alloys.

The dissimilar AA5083/AA6083 FSW joint was sampled in two different directions, transverse and longitudinal, to assess the characteristics of the joint [13]. The aim was to analyze the variations by comparing these samples taken from different orientations with the parent materials through macro/microstructure, tensile, and micro-hardness tests. The findings indicated that the transverse samples had a hardness value of 93.90 HV0.2, while the longitudinal samples had a higher value of 119.27 HV0.2. Similarly, the transverse samples exhibited the highest tensile strength of 130.694 MPa with a strain value of 0.054, whereas the longitudinal samples had a tensile strength of 127.833 MPa and a strain value of 0.0834. However, a study conducted by Garg et al. [14] using the finite element method focused on an FSW dissimilar joint AA6061/AA7075. The results of their study showed that the longitudinally sampled specimen exhibited a higher UTS with a lower elongation compared to the transverse specimen. Despite these differences, both sampling directions maintained a ductile fracture surface morphology.

The investigation of AA6092/SiC focused on examining the microstructure and mechanical properties, considering the direction of specimen sampling [15]. The microstructure analysis revealed distinct zones within the cross-weld specimen, including the base metal, heat-affected zone, thermo-mechanically affected zone, and stir zone. On the other hand, the longitudinal specimen exhibited a fine equiaxed grain structure. In terms of tensile strength, the longitudinal specimen demonstrated both higher ductility and strength compared to the transverse specimen, which aligns with common observations in similar joints. Additionally, the hardness behavior exhibited a similar pattern to the tensile strength, attributed to the grain refinement in the longitudinal specimen.

The sampling direction in friction stir welding of dissimilar aluminum alloys holds significant importance, alongside other crucial factors, for maximizing its application. Specimens can be sampled either perpendicular or longitudinal to the weld direction. Cutting the specimens longitudinally (parallel to the direction of the joint) FSW of dissimilar aluminum alloys provides valuable information about the weld characteristics, aids in understanding the welding process, facilitates mechanical property evaluation and contributes to process optimization in dissimilar aluminum alloys. However, it is important to note that the

specific novelty and significance of this approach may vary depending on the context and the research study or development being referred to.

This paper investigates the influence of sampling direction on the microstructure and mechanical properties of dissimilar aluminum alloy joints fabricated via friction stir welding.

2. Materials and Methods

This study employed two aluminum alloy grades: AA6082-T651 and AA8011-H14 plates, both with a thickness of 6 mm. The chemical composition of these alloys is provided in Table 1, while Table 2 displays their corresponding mechanical properties. The plates were cut into dimensions of 55 × 265 mm to align with the FSW fixture bed used. The FSW process was carried out using a converted LAGUN FU. 1-LA conventional universal milling machine manufactured by the LAGUN MACHINE TOOLS S.L.U. in Gipuzkoa in Spain.

In Figure 1a, a photograph of the FSW tool utilized in the study is depicted, accompanied by comprehensive tool parameters as outlined in Table 3. In addition to Table 3, it should be noted that the penetration depth is the same as the pin length, which is 5.7 mm down into the materials. To determine the FSW parameters, the Taguchi L9 method was employed [16]. The FSW setup is depicted in Figure 1b,c showcases the resulting dissimilar joint produced by FSW. Following the FSW process, test specimens were obtained from the joint, considering two sampling directions: transverse (trans) and longitudinal (long). The sampling directions are visualized in Figure 1d, with dimensions in mm.

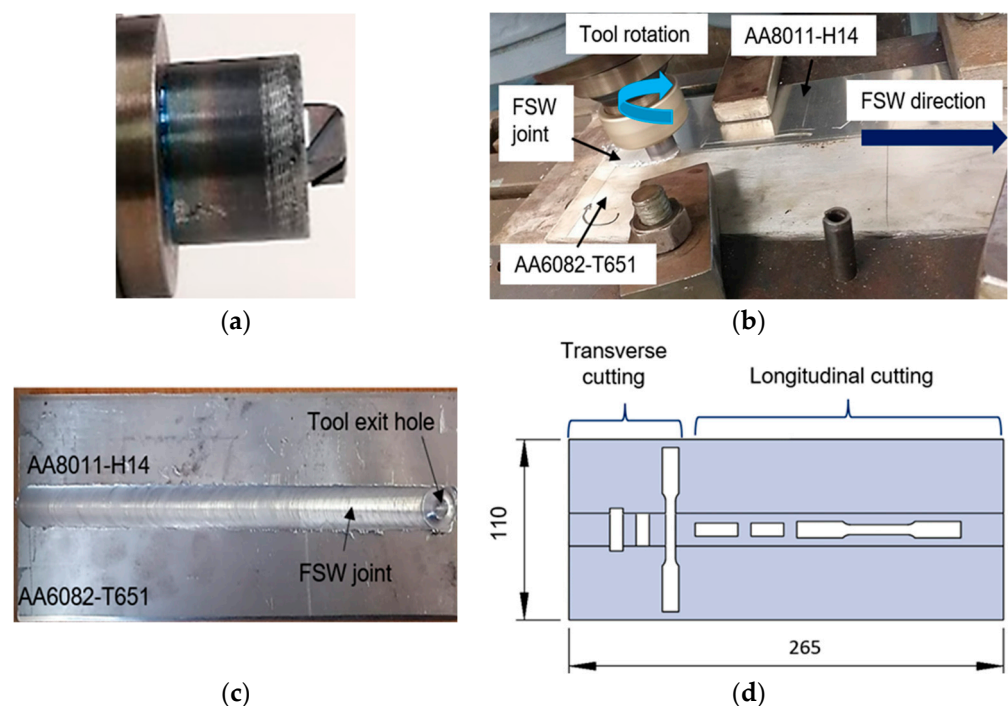


Figure 1. (a) FSW tool, (b) FSW process, (c) FSW produced joint, and (d) sampling direction.

Table 1. Chemical composition of the materials (wt %) [17].

	Mg	Zn	Ti	Cr	Si	Mn	Fe	Ni	Cu	Al
AA6082-T651	1.23	0.51	0.04	0.00	1.24	0.38	0.72	0.11	0.03	Balance
AA8011-H14	0.55	0.63	0.03	0.03	0.38	0.76	1.33	0.12	0.06	Balance

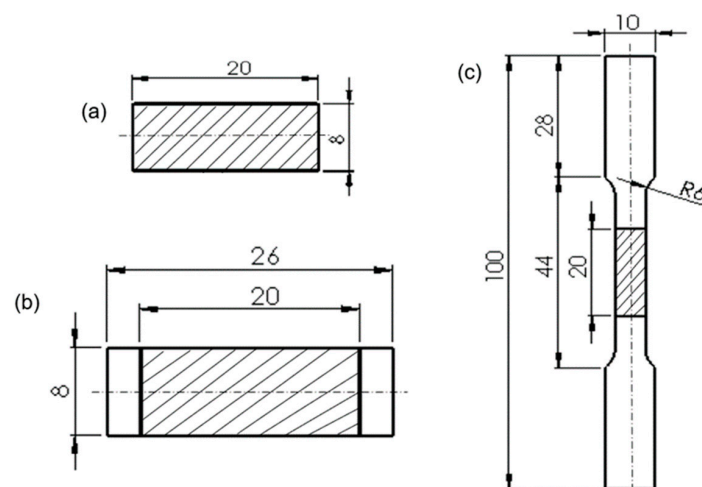
Table 2. Mechanical properties of the materials [18].

Property	Material	
	AA6082-T651	AA8011-H14
Yield strength (MPa)	270	76
Tensile strength (MPa)	307.5	94.1
Elongation (%)	26.22	40.17
Hardness (HV)	90	34

Table 3. FSW tool parameters [16].

Material	Pin Length (mm)	Pin Diameter (mm)	Tilt Angle (°)	Shoulder Diameter (mm)	Shoulder Length (mm)	Traverse Speed (mm/min)	Rotational Speed (rpm)
High-speed steel	5.7	7	2	20	15	60	1100

The conducted tests encompassed various analyses, including microstructural analysis, X-ray diffraction (XRD) analysis, tensile tests, microhardness tests, and fractographic analysis. For the dissimilar friction stir welded (FSW) joints, the chemical composition analysis was performed to determine the phases present in the XRD analysis. The specimen used for chemical and XRD analysis is depicted in Figure 2a. The Belec Compact Spectrometer HLC (Belec Spectrometry Opto-Electronics GmbH, Georgsmarienhütte, Germany) machine, utilizing high-purity Argon gas (99.99%), was employed to detect the chemical composition of the produced FSW dissimilar joints. The Belec WIN 21 software, integrated into the Belec machine, was utilized to measure the chemical composition.

**Figure 2.** (a) XRD specimen—top view, (b) microstructure—top view specimen, and (c) tensile specimen (all dimensions in mm).

Subsequently, the XRD analysis was carried out on the samples following the chemical composition analysis, and the services of iThemba Laboratory Solutions company were utilized. A Bruker D8-Advance multi-purpose X-ray diffractometer manufactured by the Bruker Corporation, Massachusetts based in the United States was employed for the XRD measurements. The instrument operated in continuous θ - θ scan mode with locked coupling, employing Cu-K α radiation. The measurement range in 2θ was determined by the user, with a typical step size of 0.034° . The diffraction data were recorded using a position-sensitive detector called Lyn-Eye, with a typical speed of 0.5 s/step, which is equivalent to an effective time of 92 s/step for a scintillation counter. The background of the data was subtracted to obtain diffraction patterns with zero background. A set of potential elements from the periodic table was selected for phase analysis, and phases were

identified by comparing the calculated peaks with the measured ones until all phases were identified within the resolution limits of the results.

The microstructural analysis was conducted in accordance with the ASTM E112-12 standard [19]. Cut-off specimens were mounted using hot mounting resin to prepare the specimens for microstructure analysis. Figure 2b displays the dimensions of the microstructure specimen. After mounting, the specimens underwent grinding, polishing, and subsequent etching using Weck's and Modified Keller's etchants. For Weck's etchant, a chemical mixture containing 4 g of potassium permanganate, 1 g of sodium hydroxide, and distilled water was applied to the specimens for a duration of 15 s. Modified Keller's etchant consisted of 10 mL of nitric acid, 1.5 mL of hydrochloric acid, 1.0 mL of hydrofluoric acid, and 87.5 mL of distilled water. It was applied to the joints for 20 s following Weck's etchant.

Following the etching process, microstructural images of the FSW joints were captured using the Motic AE2000 MET Trinocular 100W metallurgical light optical microscope and the Motic Images Plus 3.0 software. The microscope used in this study is manufactured by The Motic Europe S.L.U. based in Barcelona in Canada. The images were taken using a 5× objective lens for base material analysis, while a 20× objective lens was used for the stir zones. The captured images were later measured using the line intercept method in ImageJ software.

The tensile tests were conducted utilizing the Hounsfield 50 K tensile testing machine, following the guidelines of the ASTM E8M-04 standard for specimen geometry and testing [20]. The diagram of the tensile specimen can be seen in Figure 2c. For Vickers microhardness testing, the Falcon 5000 Innovatest hardness testing machine is manufactured by the INNOVATEST Europe BV Manufacturing based in Maastricht in the Netherlands. The said machine is equipped with IMPRESSIONS™ software was employed. The hardness testing was carried out in accordance with the ASTM E384-11 standard [21]. The specific settings included a load of 0.3 kg, a 1 mm interval between the indents, and a total of 25 measurement indents recorded per joint. During setup, the 10× and 20× objectives were utilized for specimen focusing.

3. Results and Discussion

Figure 3 shows the XRD patterns for the FSW-Trans and FSW-Long specimens; for both XRD peaks, the presence of aluminum (α -Al), which was the dominant phase noted in both figures, is denoted by the pink dotted lines. Additional phases noted were the magnesium silicon (Mg_2Si), which is a strengthening precipitate originating from AA6082-T651 alloy [22], with the $Mg_{2.7}Fe$ and the Al_7Mn_4Fe being the iron interface base phases originating from the AA8011-H14 alloy. The iron phases, such as the Mg_2Si , are responsible for preserving the joint characteristics [23]. In light of the phases mentioned, joint failure can only result from the aluminum phase [24].

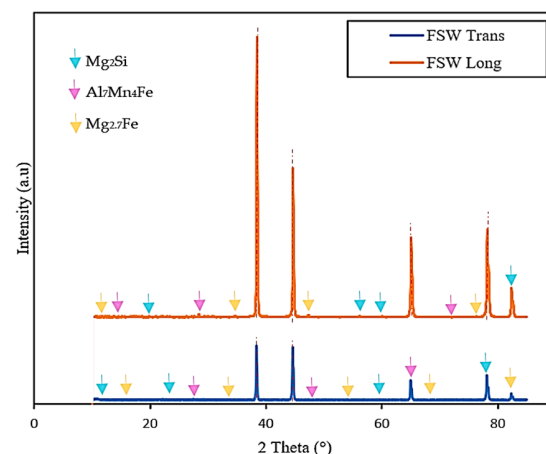


Figure 3. XRD phases for FSW-Trans and FSW-Long.

Figure 4 shows the macrographs for the FSW-Trans and FSW-Long joints. Figure 4a shows the traditional features of the FSW joint, being the single oval-shaped stir zone bands, which are commonly referred to as the onion ring structures [25,26]. The formation of the onion rings is caused by the geometric effect, which is a result of cylindrical sheets of material extruded from the retreating side of the tool during tool rotation and cutting through the sections of the two aluminum alloys [27,28]. A tunnel defect was noted as well, denoted by the red arrows. Tunnel defects are not surprising in the FSW of dissimilar material welds and are linked to insufficient heat input and signify that the tool might have traversed ahead of the welding direction before sufficient materials were deposited behind as it traversed, thereby creating a void. The void produced manifests itself in the form of a tunnel defect which plays a part in the degradation of the mechanical properties of the joint [29,30]. Comparing Figure 4b to Figure 4a, which is basically a longitudinal view of the same joint, the tunnel defect noted previously now manifests itself in the form of a line from one end to the next, denoted by the red arrow. Figure 4b appears similar to two sandwich stacked layers. These layers are identified by layer 1 (L1) and layer 2 (L2), which suggest that the microstructural arrangement in these layers may differ, thereby giving the interest to focus on microstructure examination between the two.

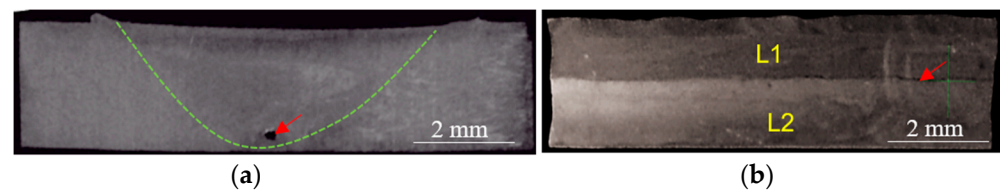


Figure 4. Macrographs, (a) FSW-Trans, and (b) FSW-Long.

Figure 5 shows the micrographs of the FSW joints produced—Figure 5a,b present the AA6082-T651 and AA8011-H14 base materials. The mean grain sizes of the two alloys were found to be 69.98 and 53.61 μm . The results obtained correlate with those reported in the literature [31]. Figure 5c shows the FSW-Trans stir zone microstructure with a mean grain size of 18.38 μm . Figure 5d depicts the FSW-Long zone, which was found to exhibit a microstructure with four layers showing the material flow of the said region. The stir zone microstructure of the FSW-Long exhibited layers in a wave-like shape due to the material mixing process during FSW. This wave-like pattern arises from the rotation and translation of the FSW tool as it traverses along the joint line. The tool exerts heat and mechanical pressure on the material, causing it to soften and mix together [32].

The stacked wave-like shape is formed by alternating regions of different material mixing concentrations. These regions represent distinct layers where the original base materials and the mixed materials are present in varying proportions. The wave-like pattern typically consists of multiple peaks and troughs, indicating areas of higher and lower mixing concentrations of the two dissimilar alloys. The presence of four different material mixing concentrations suggests that the FSW process has created four distinct layers within the stir zone of the joint. Each layer represents a combination of the original base materials and the stirred material, with varying degrees of mixing. The specific number and distribution of these layers can depend on factors such as the welding parameters, tool design, and the properties of the base materials [33,34].

However, from the four layers, two highly dominating layers were noted, those being layers L1 and L2, where the mean grain sizes were found to be 17.44 and 16.29 μm , respectively. Comparing the mean grain sizes, it was discovered that post-FSW, the grain sizes were greatly refined and equiaxed. This change was brought about by the dynamic recrystallization of the joint stir zone, where the maximum plastic deformation and thermal softening altered the grain structure completely [35,36].

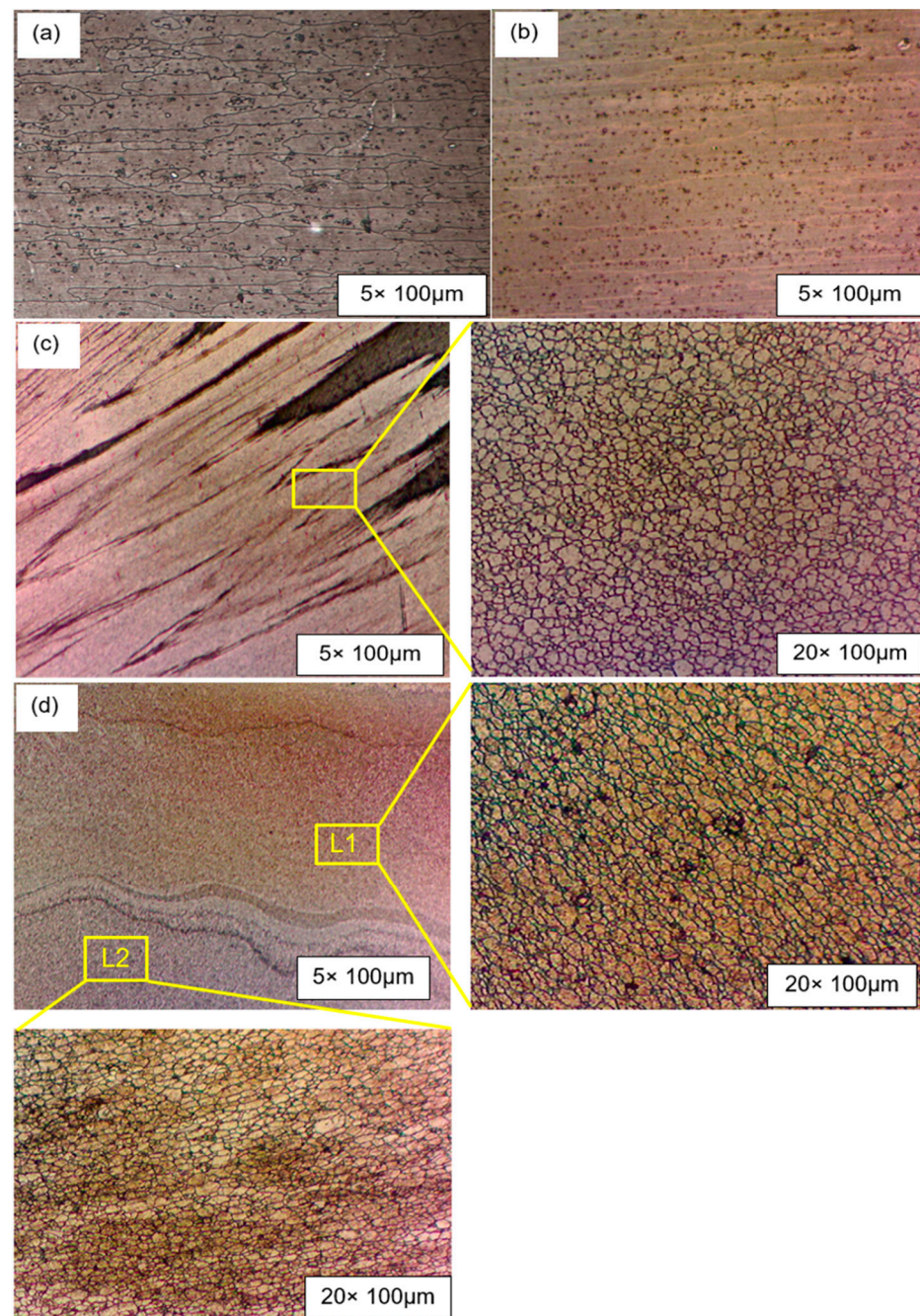


Figure 5. Base material micrographs, (a) AA6082-T651 BM, (b) AA8011-H14; stir zone micrographs, (c) FSW-Trans, and (d) FSW-Long.

Figure 6 depicts the post-tensile test specimens and produced tensile stress-strain curves with corresponding summarized tensile properties of the same in Table 4. Examining the post-tensile specimens, the stir zone (SZ) positions of fractures were noted for both specimens. The position of the fracture was influenced by the presence of the tunnel defect, as previously discussed in the macrostructural examination. Then, the tunnel defect made the stir zone the most likely region of failure [16]. Examining Figure 6c, the FSW-Long inhibited a higher ultimate tensile strength (UTS) than the FSW-Trans. Similarly, the tensile strain (elongation) followed the same behavior. This behavior is due to the FSW-Long only consisting of the stir zone material with uniform grain sizes, unlike the FSW-Trans specimen consisting of the four regions: base material, heat affected zone, thermo-mechanically affected zone, and the stir zone. An additional factor contributing to

the observed increased UTS is the presence of positive residual stress in the longitudinal direction, which is greater than that in the transverse direction. Consequently, when the samples are cut along the longitudinal direction, they have the ability to release a larger amount of residual stress compared to the transverse direction. This phenomenon likely contributes to the attainment of higher strength levels in the longitudinal direction [37,38]. Additionally, in the longitudinal joint, the applied tensile load was primarily along the direction of the weld, resulting in a more direct and uniform strain distribution [15]. The uniform strain distribution promoted better load sharing among grains and contributed to higher UTS and elongation compared to the transverse joint, where the strain was distributed less uniformly.

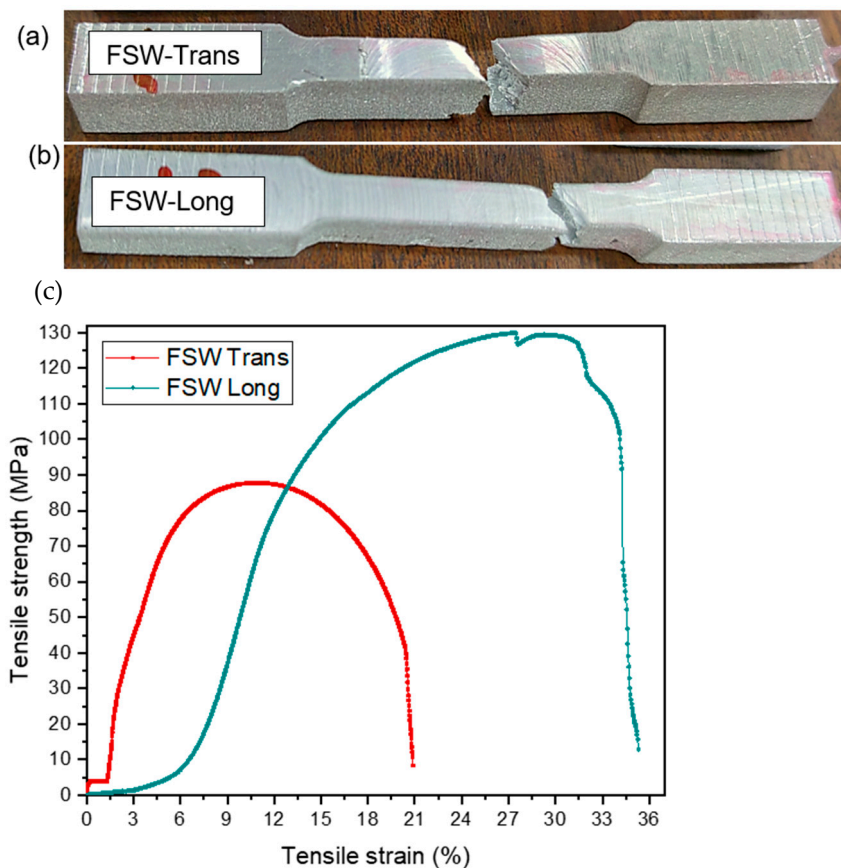


Figure 6. (a) FSW-Trans specimen, (b) FSW-Long specimen, and (c) tensile stress-strain curves.

Table 4. Tensile properties.

Weld Joint	Ultimate Tensile Strength (MPa)	Tensile Strain at UTS (%)	Tensile Strain at Breakpoint (%)	Position of Fracture
FSW Trans	88.53	14.89	27.49	SZ
FSW Long	129	27.38	35.23	SZ

Figure 7 shows the fractography of the FSW-Trans and FSW-Long joints. Both joints, while subjected to fractographic analysis to determine the nature of the fracture, displayed ductile fracture behaviour. This behaviour can be noted in the mentioned figure where the ductile fracture features were noted, those being equiaxed micro dimples, grain boundaries, microvoids, torn ridges, and transgranular cleavage facets [39–42]. Figure 8 shows the microhardness profiles of the FSW joints. The microhardness was analyzed similarly to the microstructure hence the similar labelling. From the figure, it was noted that the FSW-Trans microhardness showed a profile where the curve started from the AA6082-T651 alloy, heat-affected zone, thermo-mechanically affected zone, stir zone, then to the AA8011-H14

alloy. The obtained mean stir zone microhardness was found to be 44.65 HV. The FSW-Long L1 mean microhardness was 35.48 HV and 81 HV for the FSW-Long L2. It should be noted that the FSW-Long joint only consists of stir zone material. However, when studying the microhardness values obtained from layer 1 and layer 2, it was noted that layer 1 was dominated mainly by the AA8011-H14 alloy than the AA6082-T651 alloy. Layer 2, on the other side, consisted mostly of the AA6082-T651 rather than the AA8011-H14 alloy. The behaviour of the microhardness was found to correlate with the grain sizes of the mentioned regions [43,44].

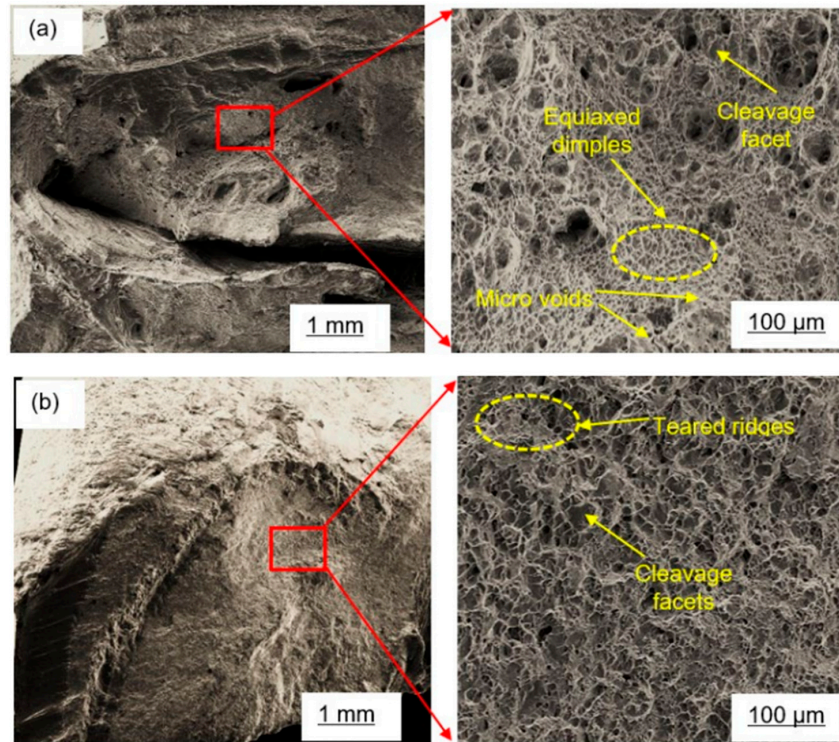


Figure 7. Fractography, (a) FSW-Trans, and (b) FSW-Long.

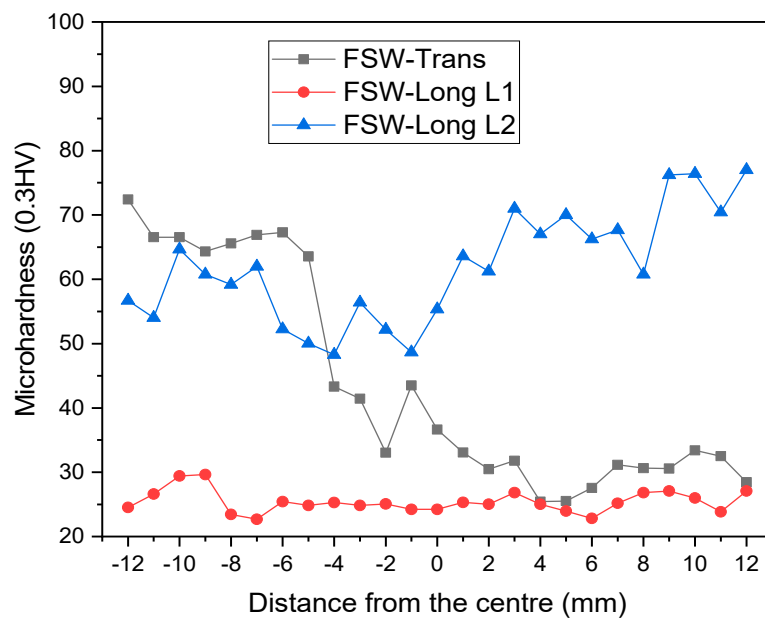


Figure 8. Microhardness profiles.

4. Conclusions

The investigation into the microstructure and mechanical properties of friction stir welded dissimilar aluminum alloy joints based on the sampling direction yielded several significant conclusions:

Firstly, the X-ray diffraction analysis indicated that aluminum was the predominant phase in the joints, accompanied by strengthening phases such as magnesium silicon and magnesium iron.

A notable observation emerged from the microstructure analysis, revealing a distinct difference between the FSW longitudinal and transverse joints. The FSW longitudinal joint exhibited a stacked sandwich-like microstructure, while the FSW transverse joint displayed a banded onion ring microstructure.

The microhardness measurements further demonstrated variations between the two joint types. The FSW transverse dissimilar joints exhibited a microhardness of 44.65 HV, whereas the FSW longitudinal joint displayed a more complex microstructural arrangement consisting of two layers. Layer 1 had a mean microhardness of 35.48 HV, while layer 2 exhibited a microhardness of 81 HV. These microhardness values aligned with the respective grain sizes observed in the joints. It is worth elaborating that FSW introduced significant plastic deformation and stirring action, leading to grain refinement in the welded zone. In the longitudinal joint, the direction of grain flow is aligned with the loading direction during hardness testing, resulting in a more direct load transmission through the grains. This alignment contributed to higher microhardness values in the longitudinal direction compared to the transverse direction, where the load may encounter a less direct path through the grains.

Furthermore, the ultimate tensile strength of the FSW longitudinal joints surpassed that of the FSW transverse joints. The FSW longitudinal joints exhibited a tensile strength of 129.9 MPa, whereas the FSW transverse joints achieved a lower tensile strength of 88.5 MPa. A similar trend was observed for elongation, with the FSW longitudinal joints demonstrating a higher tensile strain of 35.32% compared to the 20.89% tensile strain observed in the FSW transverse joints. This behavior was due to the strain and residual stresses experienced during tensile loading.

Fractographic analysis indicated that all the joints exhibited a ductile fracture behavior when subjected to mechanical testing, further supporting the presence of favorable mechanical properties.

In conclusion, the investigation successfully explored the microstructure and mechanical properties of friction stir welded dissimilar aluminum alloy joints based on the sampling direction. The findings highlighted the distinctive microstructural differences, variations in microhardness, ultimate tensile strength, and elongation between the FSW longitudinal and transverse joints. These insights contribute to a deeper understanding of the joint characteristics and performance, aiding in the development and optimization of friction stir welding processes for dissimilar aluminum alloy joints.

Author Contributions: Conceptualization, S.M. and V.M.; methodology, S.M.; software V.M.; validation, S.M. and V.M.; formal analysis, S.M.; investigation, S.M.; resources, V.M.; data curation, S.M.; writing—original draft preparation, S.M.; writing—review and editing, V.M.; visualization, S.M.; supervision, V.M.; project administration, S.M.; funding acquisition, V.M. All authors have read and agreed to the published version of the manuscript.

Funding: This research is funded by the SOUTH AFRICAN NATIONAL RESEARCH FOUNDATION—THUTHUKA GRANT 138268.

Data Availability Statement: Data is available upon request.

Acknowledgments: The authors would like to thank the Cape Peninsula the University of Technology, Department of Mechanical and Mechatronic Engineering workshop staff for their sincere support during the fabrication and testing of the joints and Miranda Waldron from the University of Cape Town for assistance with the SEM tests. Special gratitude also goes to Remi Butcher from the iThemba Labs for assistance analyzing the XRD samples.

Conflicts of Interest: The authors declare no conflict of interest.

References

1. Mishra, R.S.; De, P.S.; Kumar, N. *Friction Stir Welding and Processing*; Springer: Berlin, Germany, 2014; pp. 259–296.
2. Mishra, R.S.; Ma, Z.Y. Friction stir welding and processing. *Mater. Sci. Eng. R Rep.* **2005**, *50*, 1–78. [[CrossRef](#)]
3. Zhang, Y.N.; Cao, X.; Larose, S.; Wanjara, P. Review of tools for friction stir welding and processing. *Canad. Metall. Q.* **2012**, *51*, 250–261. [[CrossRef](#)]
4. Varunraj, S.; Ruban, M. Investigation of the microstructure and mechanical properties of AA6063 and AA7075 dissimilar aluminium alloys by friction stir welding process. *Mater. Today Proc.* **2022**, *68*, 1654–1657. [[CrossRef](#)]
5. Gowthaman, P.S.; Saravanan, B.A. Determination of weldability study on mechanical properties of dissimilar Al-alloys using friction stir welding process. *Mater. Today Proc.* **2021**, *44*, 206–212. [[CrossRef](#)]
6. Kailainathan, S.; Sundaram, S.K.; Nijanthan, K. Influence of friction stir welding parameter on mechanical properties in dissimilar aluminium alloys. *Int. J. Innov. Res. Sci. Eng. Technol.* **2014**, *3*, 15691–15695. [[CrossRef](#)]
7. Guo, J.F.; Chen, H.C.; Sun, C.N.; Bi, G.; Sun, Z.; Wei, J. Friction stir welding of dissimilar materials between AA6061 and AA7075 Al alloys effects of process parameters. *Mater. Des.* **2014**, *56*, 185–192. [[CrossRef](#)]
8. Khanna, N.; Sharma, P.; Bharati, M.; Badheka, V. Friction stir welding of dissimilar aluminium alloys AA 6061-T6 and AA 8011-h14: A novel study. *J. Braz. Soc. Mech. Sci. Eng.* **2020**, *42*, 7. [[CrossRef](#)]
9. Karimi, N.; Nourouzi, S.; Shakeri, M.; Habibnia, M.; Dehghani, A. Effect of tool material and offset on friction stir welding of Al alloy to carbon steel. *Adv. Mater. Res.* **2012**, *445*, 747–752.
10. Palani, K.; Elanchezian, C.; Avinash, K.; Karthik, C.; Chaitanya, K.; Sivanur, K.; Reddy, K.Y. Influence of friction stir processing parameters on tensile properties and microstructure of dissimilar AA 8011-h24 and AA 6061-t6 aluminum alloy joints in nugget zone. *IOP Conf. Ser.* **2018**, *390*, 012108. [[CrossRef](#)]
11. Cole, E.G.; Fehrenbacher, A.; Duffie, N.A.; Zinn, M.R.; Pfefferkorn, F.E.; Ferrier, N.J. Weld temperature effects during friction stir welding of dissimilar aluminum alloys 6061-T6 and 7075-T6. *Int. J. Adv. Manuf. Technol.* **2014**, *71*, 643–652. [[CrossRef](#)]
12. Rani, N.; Bishnoi, R.N.; Mahendru, A. Effect of tool pin profile on mechanical properties of single pass and double pass friction stir welded aluminium alloys AA6061 & AA8011. *Int. J. Curr. Eng. Technol.* **2015**, *5*, 3780–3783.
13. Segaetsho, M.O.M.; Msomi, V.; Moni, V. A comparative analysis between the transverse and longitudinal samples of the FSW AA5083/AA6082 Joints. *Key Eng. Mater.* **2023**, *944*, 3–12. [[CrossRef](#)]
14. Garg, A.; Raturi, M.; Bhattacharya, A. Experimental and finite element analysis of progressive failure in friction stir welded AA6061-AA7075 joints. *Procedia Struct. Integr.* **2019**, *17*, 456–463. [[CrossRef](#)]
15. Omar, S.S.; Hengan, O.U.; Xingguo, W.; Sun, W. Microstructure and mechanical properties of friction stir welded AA6092/SiC metal matrix composite. *Mater. Sci. Eng. A* **2019**, *742*, 78–88.
16. Msomi, V.; Mabuwa, S. Optimization of Normal and Submerged FSP Parameters for dissimilar aluminium joints using Taguchi technique. *MSF* **2023**, *1034*, 207–218.
17. Msomi, V.; Mabuwa, S.; Merdji, A.; Muribwathoho, O.; Motshwanedi, S.S. Microstructural and mechanical properties of submerged multi-pass friction stir processed AA6082/AA8011 TIG-welded joint. *Mater. Today Proc.* **2021**, *45*, 5702–5705. [[CrossRef](#)]
18. Mabuwa, S.; Msomi, V. The impact of submerged friction stir processing on the friction stir welded dissimilar joints. *Mater. Res. Express* **2020**, *7*, 096513. [[CrossRef](#)]
19. ASTM International. Standard Test Methods for Determining Average Grain Size (ASTM E112-12). 2012; pp. 1–27. Available online: <https://www.astm.org/Standards/E112.htm> (accessed on 28 June 2023).
20. ASTM International. Standard Test Methods for Tension Testing of Metallic Materials (ASTM E8M-04). 2004; pp. 1–24. Available online: <https://www.astm.org/Standards/E8M.htm> (accessed on 28 June 2023).
21. ASTM International. Standard Test Method for Microindentation Hardness of Materials (ASTM E384-11). 2011; pp. 1–24. Available online: <https://www.astm.org/Standards/E384.htm> (accessed on 28 June 2023).
22. Balakrishnan, M.; Dinaharan, I.; Palanivel, R.; Sathiskumar, R. Effect of friction stir processing on microstructure and tensile behavior of AA6061/Al3Fe cast aluminum matrix composites. *J. Alloys Comp.* **2019**, *785*, 531–541.
23. Mvola, B.; Kah, P.; Martikainen, J. Welding of dissimilar non-ferrous metals by GMAW processes. *Int. J. Mech. Mater. Eng.* **2014**, *9*, 1–11. [[CrossRef](#)]
24. Tan, L.; Katoh, Y.; Tavassoli, A.A.F.; Henry, J.; Rieth, M.; Sakasegawa, H.; Tanigawa, H.; Huang, Q. Recent status and improvement of reduced-activation ferritic martensitic steels for high-temperature service. *J. Nucl. Mater.* **2016**, *479*, 515–523. [[CrossRef](#)]
25. Chen, H.B.; Yan, K.; Lin, T.; Chen, S.B.; Jiang, C.Y.; Zhao, Y. The investigation of typical welding defects for 5456 aluminum alloy friction stir welds. *Mater. Sci. Eng. A* **2006**, *433*, 64–69. [[CrossRef](#)]

26. Palani, K.; Elanchezian, C.; Vijaya Ramnath, B.; Bhaskar, G.B.; Naveen, E. Effect of pin profile and rotational speed on microstructure and tensile strength of dissimilar AA8011, AA01-T6 friction stir welded aluminum alloys. *Mater. Today Proc.* **2018**, *5*, 24515–24524. [[CrossRef](#)]
27. Mehdi, H.; Mishra, R.S. Effect of friction stir processing on mechanical properties and wear resistance of tungsten inert gas welded joint of dissimilar aluminum alloys. *J. Mater. Eng. Perform.* **2021**, *30*, 1926–1937. [[CrossRef](#)]
28. Mohammadzadeh, H.J.; Farahani, H.; Besharati, M.K.G.; Aghaei, M.V. Study on the effects of friction stir welding process parameters on the microstructure and mechanical properties of 5086-H34 aluminum welded joints. *Int. J. Adv. Manuf. Technol.* **2016**, *83*, 611–621. [[CrossRef](#)]
29. Agha Amini Fashami, H.; Bani Mostafa Arab, N.; Hoseinpour Gollo, M. Numerical and experimental investigation of defects formation during friction stir processing on AZ91. *SN Appl. Sci.* **2021**, *3*, 108. [[CrossRef](#)]
30. Khan, N.Z.; Siddiquee, A.N.; Khan, Z.A.; Shihab, S.K. Investigations on tunneling and kissing bond defects in FSW joints for dissimilar aluminum alloys. *J. Alloys Compd.* **2015**, *648*, 360–367. [[CrossRef](#)]
31. Mabuwa, S.; Msomi, V. The impact of material positioning towards the friction stir welded dissimilar aluminium alloy joints. *Recent Pat. Mech. Eng.* **2020**, *14*, 252–259.
32. Mabuwa, S.; Msomi, V.; Mehdi, H.; Ngonda, T. A study on the metallurgical characterization of the longitudinally sampled friction stir processed TIG welded dissimilar aluminum joints. *Proc. Inst. Mech. Eng. Part E J. Process Mech. Eng.* **2023**, 09544089231169589. [[CrossRef](#)]
33. Das, J.; Robi, P.S.; Sankar, M.R. Assessment of parameters windows and tool pin profile on mechanical property and microstructural morphology of FSWed AA2014 joints. *SN Appl. Sci.* **2020**, *2*, 1–15. [[CrossRef](#)]
34. Segaletsho, M.O.M.; Msomi, V.; Moni, V. Traverse and longitudinal analysis of AA5083/AA6082 dissimilar joint. *Eng. Res. Express* **2023**, *5*, 035004. [[CrossRef](#)]
35. He, Z.; Peng, Y.; Yin, Z.; Lei, X. Comparison of FSW and TIG welded joints in Al–Mg–Mn–Sc–Zr alloy plates. *Trans. Nonferr. Met. Soc. China* **2011**, *21*, 1685–1691. [[CrossRef](#)]
36. Peng, G.; Yan, Q.; Hu, J.; Chen, P.; Chen, Z.; Zhang, T. Effect of forced air cooling on the microstructures, tensile strength, and hardness distribution of dissimilar friction stir welded AA5A06-AA6061 joints. *Metals* **2019**, *9*, 304. [[CrossRef](#)]
37. Farhang, M.; Farahani, M.; Nazari, M.; Sam Daliri, O. Experimental correlation between microstructure, residual stresses and mechanical properties of friction stir welded 2024-T6 aluminum alloys. *Int. J. Adv. Manuf. Technol.* **2022**, *15*, 1–9.
38. Farhang, M.; Sam-Daliri, O.; Farahani, M.; Vatani, A. Effect of friction stir welding parameters on the residual stress distribution of Al-2024-T6 alloy. *J. Mech. Eng. Sci.* **2021**, *15*, 7684–7694. [[CrossRef](#)]
39. Zhao, H.J.; Wang, B.Y.; Liu, G.; Yang, L.; Xiao, W.C. Effect of vacuum annealing on microstructure and mechanical properties of TA15 titanium alloy sheets. *Trans. Nonferr. Met. Soc. China* **2015**, *25*, 1881–1888. [[CrossRef](#)]
40. Dragatogiannis, D.A.; Koumoulos, E.P.; Kartsonakis, I.; Pantelis, D.I.; Karakizis, P.N.; Charitidis, C.A. Dissimilar friction stir welding between 5083 and 6082 Al alloys reinforced with TiC nanoparticles. *Mater. Manuf. Process.* **2016**, *31*, 2101–2114. [[CrossRef](#)]
41. Msomi, V.; Moni, V. The influence of materials positioning on microstructure and mechanical properties of friction stir welded AA5083/AA6082 dissimilar joint. *Adv. Mater. Process. Technol.* **2021**, *8*, 2087–2101. [[CrossRef](#)]
42. Pouraliakbar, H.; Beygi, R.; Fallah, V.; Monazzah, A.H.; Jandaghi, M.R.; Khalaj, G.; Da Silva, L.F.M.; Pavese, M. Processing of Al-Cu-Mg alloy by FSSP: Parametric analysis and the effect of cooling environment on microstructure evolution. *Mater. Lett.* **2022**, *308*, 131157. [[CrossRef](#)]
43. Ravikumar, S.; Seshagiri-Rao, V.; Pranesh, R.V. Effect of welding parameters on macro and microstructure of friction stir welded butt joints between AA7075-T651 and AA6061-T651 alloys. *Proc. Mater. Sci.* **2014**, *5*, 1725–1735.
44. Li, K.; Liu, X.; Zhao, Y. Research status and prospect of friction stir processing technology. *Coatings* **2019**, *9*, 129. [[CrossRef](#)]

Disclaimer/Publisher’s Note: The statements, opinions and data contained in all publications are solely those of the individual author(s) and contributor(s) and not of MDPI and/or the editor(s). MDPI and/or the editor(s) disclaim responsibility for any injury to people or property resulting from any ideas, methods, instructions or products referred to in the content.